

Clare M.C. Tempany and Gabor Fichtinger

Introduction

Imaging plays a major role in the detection, diagnosis, and staging of cancer. In fact, many cancers, such as renal cell carcinoma and breast cancer, are uniquely diagnosed and staged by standard imaging modalities including computed tomography (CT) scans or mammography. These imaging studies when used appropriately have led to early detection, reduced the lead time in diagnosis and treatment, and ultimately saved many lives. This chapter will outline our approach to attempting to bring a rational and pragmatic image-guided approach to the diagnosis and treatment of prostate cancer. First, we will discuss the use of prostate magnetic resonance (MR) imaging to detect suspicious foci and direct sampling under either MRI or combined transrectal ultrasound (TRUS) and MRI guidance. The latter could resolve a major clinical dilemma by providing combined pre-biopsy imaging and image-directed targeted sampling of the gland. Secondly, in treatment protocols, MRI has allowed the introduction of subtotal gland therapies; for example, MRI-guided brachytherapy or MRI-guided ablative focal therapy, such as focused ultrasound (FUS), laser, and cryotherapy.

C.M.C. Tempany, MD (✉)
National Center for Image Guided Therapy,
Department of Radiology,
Brigham and Women's Hospital,
Harvard Medical School, Boston, MA, USA
e-mail: ctempnyafdhal@partners.org,
ctempny@bwh.harvard.edu

G. Fichtinger, PhD
Queen's University, School of Computing,
25 Union Street, Kingston, ON K7L 3N6, Canada
e-mail: gabor@cs.queensu.ca

Background on Clinical Issues of Prostate Cancer

The current workup in the detection of prostate cancer is relatively primitive and consists of a direct palpation examination through the rectum, which is inherently subjective, and a blood test to measure the serum prostate-specific antigen (PSA), the results of which may necessitate a core needle biopsy. Most experts agree however that with the widespread use of PSA and biopsy, too many men are overstaged and overtreated today. The recent NIH-funded Prostate, Lung, Colorectal, and Ovarian Cancer Screening Trial showed no difference in prostate cancer death rates between men screened and those not screened by PSA [1]. As we increasingly recognize that death rates from prostate cancer are low, the balance between cancer control and preservation of quality of life becomes even more important. The European Randomized Study [2] of Screening for Prostate Cancer compared two groups of men: one was screened with PSA every 4 years, and the other group was not. In the study, researchers measured the effects using death from prostate cancer as the outcome. They concluded that, to save one life, 1,410 men would need to be screened and 48 men treated. The public health impact of this disease is far-reaching, extending beyond cost and resource utilization. The sheer numbers of men with prostate cancer are extraordinary; according to the American Cancer Society, about 241,740 men are newly diagnosed every year in the USA with about 28,170 men then dying from the disease. Further, 1 man in 6 will be diagnosed with prostate cancer during his lifetime. As the USA "baby boomers" age, there will be an increase in prostate cancer diagnosis and the numbers of men presenting for therapy [3]. Thus the burden of overdiagnosis is very significant.

Further confounding factors in treating this prostate cancer include inequities in terms of access and type of treatment offered based on socioeconomic and racial disparities. Interestingly, a recent publication by Barbieri et al. reported on the socioeconomic differences in the UK; it compared the private sector with National Health Service (NHS) patients and found that the former have a lower probability of having advanced disease than the NHS patients with an odds ratio (*OR*) of 0.75 ($P < 0.001$), a higher probability of surgery (*OR* 1.28 $P < 0.037$), and lower radiotherapy use (or 0.75 $P < 0.001$). The study also found, even after adjusting for private sector diagnosis, substantial socioeconomic differences exist across centers in the NHS in stage and treatment patterns [4]. The lay press covers many of these issues with often conflicting messages, such as the most recent set of stories about the PSA screening controversy. For these and other reasons, many men are reluctant to seek advice as they frequently become confused as information and messages conflict when they deal with the medical profession regarding treatment options.

Prostate Cancer Diagnosis

A definitive diagnosis of prostate cancer must be made by histopathological examination of biopsy specimens that are most commonly obtained via transrectal ultrasound-guided biopsy performed in the doctor's office under local anesthesia. However, numerous studies have shown that TRUS-guided prostate biopsy misses cancer in at least 20 % of cases [5–9]. The gloomy consequence is that for this reason alone, not counting other factors, in more than 20 % of cancers, at least two biopsy sessions are required to achieve a diagnosis. This represents more than 200,000 repeat biopsy sessions annually in the USA alone. Current TRUS-guided approaches do not target a specific lesion within the prostate gland but rather take typically 12 samples/cores systematically from the gland. Finding a focal prostate cancer has been compared to “finding a needle in a haystack”. There are three current approaches to resolving this dilemma: first, the most common one is increased sampling, or so-called saturation biopsy (20–80 cores at 5-mm increments across the gland); second, the least common, is optimized TRUS and the use of an intravenous microbubble contrast enhancement (CE) agent and Doppler US [10–12]; and third, what we believe the most exciting, is the introduction of MR-guided biopsies. There are several approaches one of which is in-core transperineal targeted sampling approach pioneered by our group and now adopted by several centers [13–26]. Regrettably, the aforementioned modern TRUS approaches have not been adopted for several reasons, one being the lack of FDA clearance of the microbubble agents. A further challenge with the saturation or 3D mapping biopsies is that they require from 20 to 80 cores and are, therefore, clearly more invasive and complex than current standard biopsies given their onerous pathological analyses.

Prostate Cancer Treatment

The current management goal for clinically localized prostate cancer must be risk-assessed patient-specific treatment with minimal side effects. In diagnosing and staging prostate cancer today, imaging plays an increasingly important role. If a man has prostate cancer, the disease's overall low morbidity presents a very significant dilemma regarding treatment choice: which type, how it is delivered, and what side effects may be encountered. Currently, treatment selection is based primarily upon the clinical stage of the patient's disease and his age, comorbidities, serum PSA, and biopsy Gleason score. Men with so-called “clinically insignificant” disease with a low Gleason score of < 6 and tumor volumes of < 0.5 cc are often “treated” with active surveillance and those with “clinically significant” localized disease are being treated aggressively with either surgery or radiation.

Current treatments for localized prostate cancer are either active surveillance [27] or interventions such as either radical prostatectomy or whole-gland radiation. Radiation treatments include either brachytherapy or external beam radiation therapy (EBRT) with intensity-modulated radiation or 3D conformal external beam radiation. A less common radiation treatment is proton beam therapy, although there appears to be little to gain from the application of protons compared to the photon-based. The side effects and morbidities of all prostate cancer treatments today remain a very significant source of concern for men when choosing how to manage their disease. Thus, more and more men who meet the eligibility criteria are choosing to avoid treatment and select “active surveillance”. MRI has an important role to play in this group both initially at diagnosis and during surveillance. The initial role is to confirm that the cancer is confined to the gland and, now with multiparametric MRI (mpMRI) techniques including apparent diffusion coefficient (ADC), to detect, localize, and characterize the index lesion. The index lesion is the largest one with the highest Gleason score. The MRI at time of diagnosis and prior to treatment selection can provide unique information regarding the tumor size, location, aggression, and stage. In particular, it can be used to determine appropriateness of the patients for active surveillance. After a patient has been deemed eligible for active surveillance with low tumor volume, intermediate ADC values, and no evidence of T3 disease, MRI can be used to monitor the disease along with the serum PSA and serial biopsies.

MR Imaging of Prostate Cancer

Multiple modalities can be used to image the pelvis, and they include TRUS (Fig. 56.1), CT (Fig. 56.2), and MRI (Fig. 56.3). Only two of these are of significant value in prostate imaging, namely, MRI and TRUS. It is generally

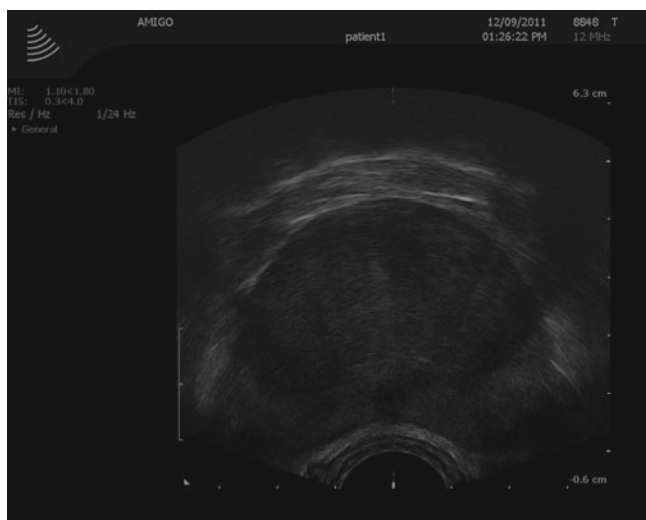


Fig. 56.1 TRUS. Transrectal ultrasound image of the prostate at the mid-gland level

agreed that MRI is the only modality capable of detecting and characterizing focal lesions in the prostate gland. Several recent reviews have outlined the current role of TRUS and MRI [28]. It is becoming increasingly evident that MRI is not only capable of sub-gland zonal imaging but can now detect and characterize focal cancer with increasing accuracy. The relatively recent introduction of 3 T MR imaging with an endorectal coil has increased the signal to noise ratio and spatial resolution of the prostate images (Fig. 56.4). Current MRI techniques involve multiple sequences, the so-called mpMRI, is most often referred to as multiparametric MRI. When multiparametric sequences are performed at 3 T with an endorectal coil, the tissue characterization capabilities are much improved over prior 1.5 T techniques. The newer sequences being used in prostate MRI include dynamic IV contrast-enhanced sequences with multiphasic imaging and pharmacokinetic analyses. Several software programs, both commercial and research, use various modeling techniques to extract tissue perfusion and detailed enhancement analyses. Perhaps the most exciting sequence being applied in prostate MRI is the diffusion-weighted imaging with multiple b values, including long ($>1,000$) values. The resulting ADC values have been found to correlate with Gleason score and they can allow clinical prognostic assessment similar to the D'Amico classification [16] of low intermediate and high risk for extra-glandular extension.

T1- and T2-Weighted MR Imaging

The techniques of T2-weighted (T2W) MRI is well established as an essential sequence, compared with other techniques, as it provides an excellent display of the prostate and

its substructure anatomy. Focal tumors usually appear as an area of low signal surrounded by the high signal of the normal peripheral zone (PZ) (Fig. 56.5). It is sometimes challenging to detect the carcinoma in the PZ due to several factors that may mimic malignant foci such as post-biopsy hemorrhage, benign prostatic hyperplasia (BPH), scars, fibromuscular tissue, calcifications, prostatitis, and the effects of radiation treatment. Even more challenging may be the detection of neoplastic tissue in the central gland where nodules appear with mixed signal intensities. If there is a homogeneous lenticular shape with low signal on T2W, a central gland focal cancer should be suspected (Fig. 56.6).

Due to its limitations, T2W alone does not achieve adequate sensitivity and specificity for detecting prostate cancer. High-signal areas in T1-weighted (T1W imaging) overlapping with low-signal areas in T2W are often likely to be artifacts due to post-biopsy hemorrhage. To avoid this error and enable better diagnostic accuracy, mpMRI techniques are now widely used, including diffusion-weighted imaging (DWI), magnetic resonance spectroscopy imaging (MRSI), dynamic contrast enhancement (DCE), and its post-processed maps; all are now part of a state-of-the-art MR imaging protocol. They can increase the detection of significant prostate cancer, markedly enabling improved diagnostic capability. The post-processed values acquired with these new techniques can be validated in several ways. For example, quantitatively using color maps that are visually easy to understand and through objective metrics such as ADC maps and parameters from two compartment pharmacokinetic models such as k_{trans} (wash in), kep (wash out), maximum slope (for wash in) and wash out, and V_e (extravascular-extracellular volume fraction), with several groups studying both approaches. Such mpMRI combined with traditional T2W can be used not only to analyze the presence or absence of prostate carcinoma and for treatment planning, but also to characterize the histological features of tumors. A study has shown that mpMRI is correlated to tissue composition for tumors and benign tissue [29], and it can allow for the differentiation between BPH and prostate cancer in the central gland [30]. The technique of mpMRI can also be used after local salvage therapy with good accuracy for determining recurrence [31].

Diffusion-Weighted MR Imaging (DWI)

First described to assess stroke and ischemia in the brain, DWI measures the water diffusion within tissue. It is well known that neoplasia, due to its local neoangiogenesis, usually affects the diffusion capacity of water molecules; therefore, this technique was translated to prostate imaging for which it provides the advantages of short acquisition times and no need for IV contrast medium administration [32]. DWI sequences are acquired using a range of b values



Fig. 56.2 CT. Multiplanar CT images of pelvis and through the prostate shows the gland boundary but no substructure detail

(500, 1,000, 1,400) to generate ADC maps. More recently, the higher b values, over 1,000, have shown great promise for the detection and characterization of focal tumors. Tumors show a lower ADC value than benign regions, both in PZ and the central gland, as Fig. 56.7 shows several studies have demonstrated the significant contribution of DWI [33–37].

It has been shown that the lower the ADC value, the higher the Gleason score and the more aggressive the tumor [38]. The addition of an ADC map to T2W images can improve the diagnostic performance of MR imaging in prostate cancer detection [39], helping the clinician to distinguish malignant from benign tissues. The combination of ADC and T2W can be used to differentiate cell density both in



Fig. 56.3 MR. (a) Transverse T2W Fast spin echo (FSE) sequence, image of the prostate at mid-gland level shows the superior signal to noise provided by 3 T with endorectal coil technique. The images show the normal high-signal peripheral zone (PZ) and mixed signals of the focal areas of benign prostatic hyperplasia (BPH) in the center.

(b) Sagittal T2W FSE shows the T2W contrast and the posterior gland surface abutting the anterior rectal wall with endorectal coil. (c) Coronal T2W FSE image of a man who has had prior brachytherapy shows the seeds, focal signal voids, and the normal appearance of the seminal vesicles superiorly

cancer and noncancerous tissue and therefore, play an important role in the estimation of the Gleason score at 3 T [36].

Dynamic Contrast-Enhanced MR Imaging

Dynamic Contrast-Enhanced MR Imaging (DCE) was introduced to effectively visualize the pharmacokinetics of gadolinium uptake in tissue as the angiogenesis of tumor differs from that of benign tissue. DCE acquires data on tissue perfusion characteristics and tumor wash-in and wash-out contrast, which are variables that rely on the pathophysiologic principle

that tumors display increased angiogenesis and, thus, are expected to show early and increased enhancement.

DCE images of the prostate are evaluated by means of the direct raw interpretation of T1W images viewed in picture archiving and computer storage (PACS) systems in static and/or cine mode (Fig. 56.8) and after processing from color maps generated from analysis by a pharmacokinetic model. The following general kinetic models are usually selected for processing: k_{trans} , k_{ep} , maximum slope for wash in and wash out, and V_e (extravascular–extracellular volume fraction). The mean peak values of k_{trans} (forward value transfer constant), k_{ep} (reverse reflux rate constant between

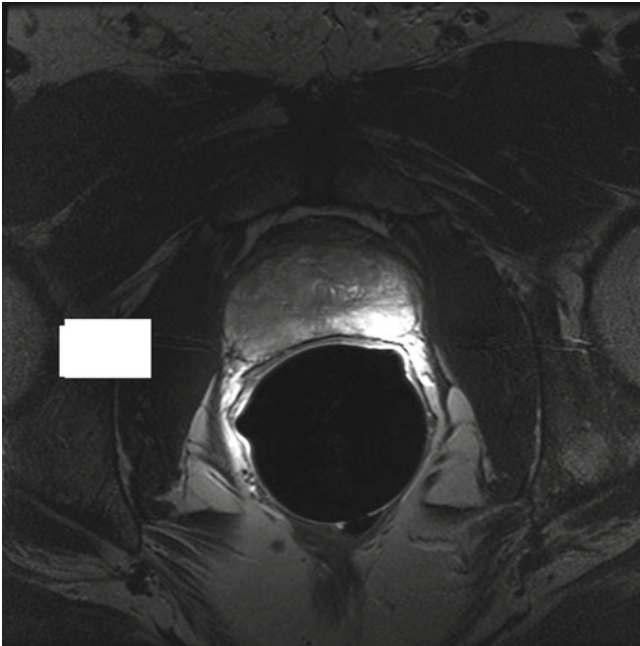


Fig. 56.4 Transverse T2W FSE image of the prostate at mid-gland level shows focal low-signal tumor on the right with normal high-signal PZ on the left

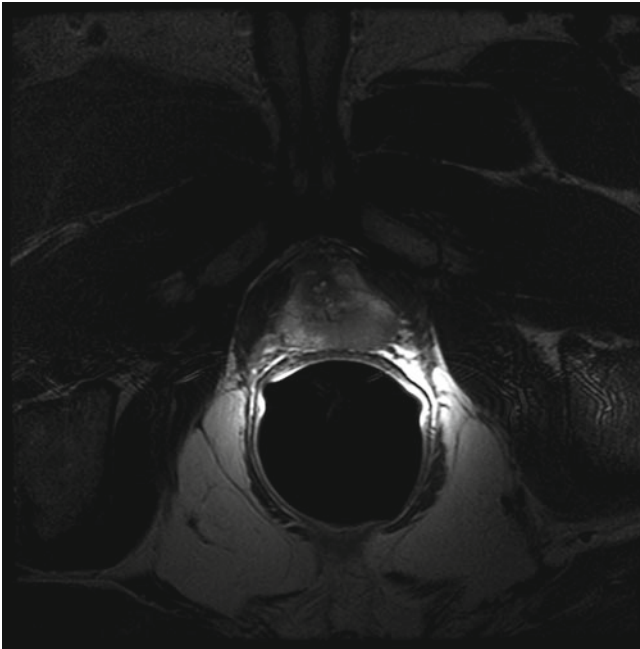


Fig. 56.5 Transverse T2W FSE image at the level of the prostate apex shows a large focal tumor on the left. Note the close proximity of the tumor to the left neurovascular bundle (NVB) on the left

extracellular space and plasma), time to peak (TTP), and maximum slope (MaxS) are currently the parameters of most common interest. These processed data can be analyzed either visually (by generating color maps) or quantitatively

through straight values. Quantitative measurements reflect some exciting results and can play an even greater role in the future of prostate care.

Prostate MRI methods may someday substitute for some of the *in vivo* assessments done today in histology. Certainly, by employing quantitative MRI, these images can be used for tumor monitoring and the assessment of treatment response. Though the difference in impact is only significant for evaluating the PZ, quantitative dynamic MRI is more accurate than T2W imaging for tumor localization of non-palpable cancer greater than 0.2 cc. Above this volume, correlation between tumor volume measured on dynamic MRI and that on the specimen is poor [29, 40]. Having said this, DCE is a proven method to help in localizing tumors within the prostate.

MR Spectroscopy Imaging

MR Spectroscopy Imaging (MRSI) is another technique that allows one to noninvasively assess metabolites present in biological tissue. Given that the use of an MRI body coil alone does not reach sufficient resolution, the endorectal coil, once introduced, changed clinical practice for the better as it made possible for 3D MRSI of the prostate with increased sensitivity. Currently, the resolution of MRSI with 1.5 T scanners is a voxel size of approximately 0.3 cm [3], while for 3 T, voxels smaller than 0.2 cm [3] are feasible. The levels of citrate, choline, and creatine have special interest for the evaluation of prostate cancer, as it is known that tumors have an elevated level of choline and a decreased level of citrate. Though it is important to point out that the graphical analysis of creatine and choline is usually not separable, the ratio (choline+creatine/citrate) can be used for the prediction of malignancy. Several studies have tried to suggest levels of these substances as predictors for prostate cancer. Kumar et al. showed a good prediction for tumor detection when a cutoff of 1.2 in (citrate/choline+creatine) ratio was used to assess the likelihood of malignancy in the PZ [41]. However, there is still no agreement among studies about metabolites concentrations as far as their abilities to suggest cancer. This lack of consensus is probably due to the differences in technique for data acquisition and interpretation; indeed, no standard has been reached. Studies have shown specificities of 49–88 % with accompanying sensitivities of 63–98 %, respectively, for MRSI. Unfortunately, most of these good results left out the analysis of the central gland. Due to signal overlapping from the PZ, MRSI still does not obtain good accuracy results in the inner regions of the gland. Moreover, a recent multi-institutional prospective study demonstrated that, compared to MRI alone, combining MRSI with MRI reaches the same levels of accuracy for detecting tumors in the PZ [42].

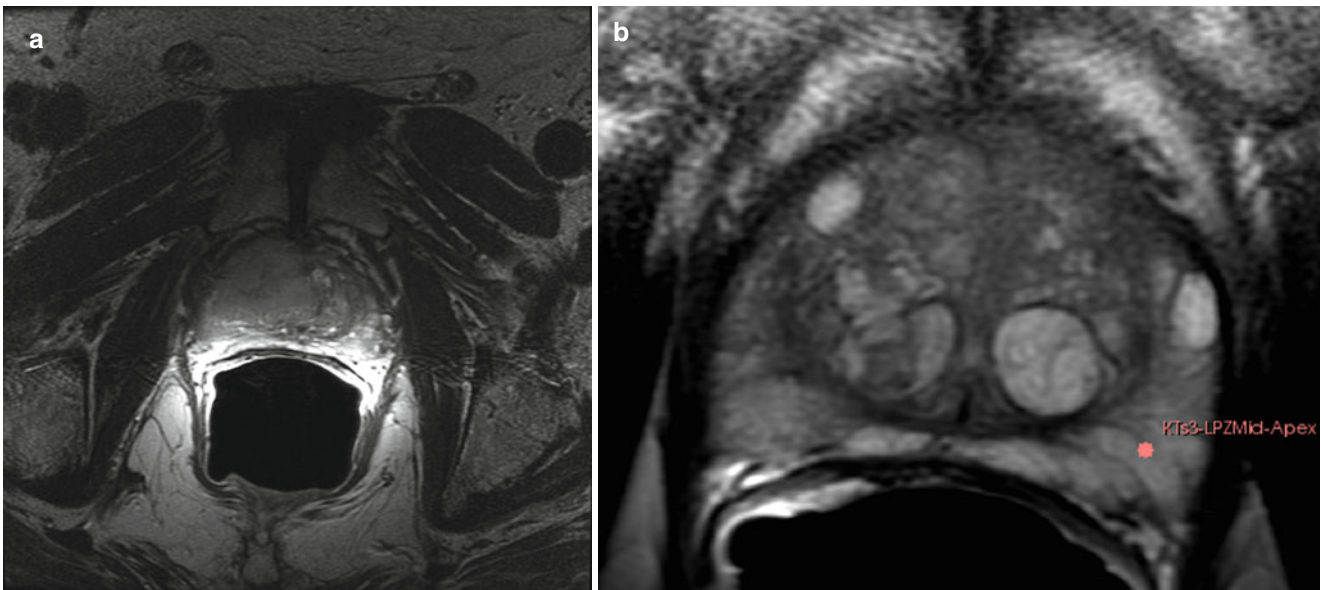


Fig. 56.6 MR imaging of prostate cancer. (a) Transverse T2W image shows a larger area of abnormal signal in both the PZ and center gland on the right. The normal BPH pattern is obliterated by the mass and a

rim of normal BPH remains on the left. (b) Pre-biopsy transverse T2W with a target on the left side. Note the excellent depiction of the PZ and BPH

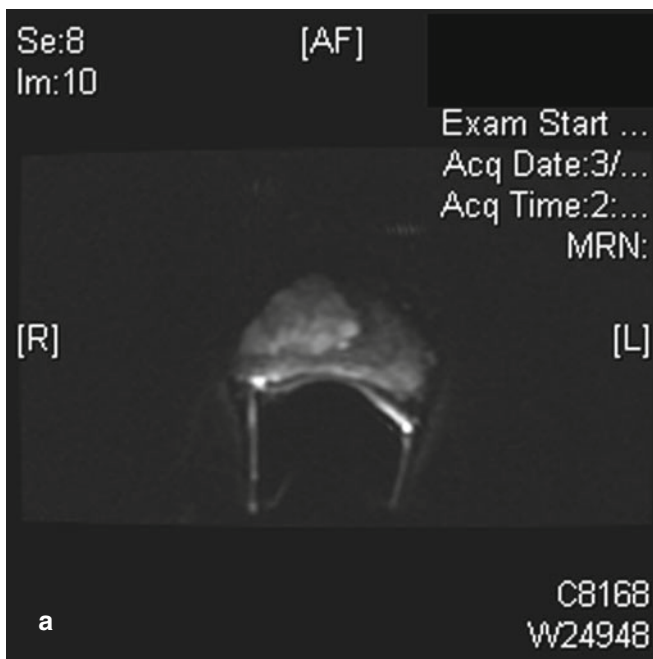
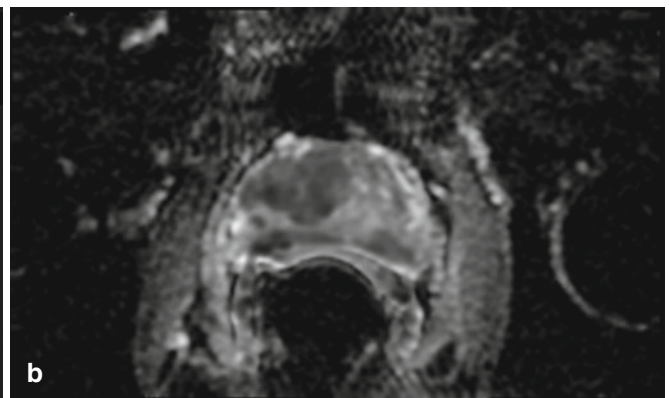


Fig. 56.7 Diffusion MR imaging of prostate cancer. (a) Transverse diffusion-weighted image (DWI) with b value of 1,400 shows a large focal area of high signal in the right gland. This was a Gleason 4+4



adenocarcinoma at pathology. (b) Same patient as (a) apparent diffusion coefficient (ADC) image shows the corresponding large area of restricted diffusion

Currently Recommended MRI Protocol for Staging

The current state-of-the-art protocol for prostate MR is to use the highest field strength available (1.5 T or greater), T1W, T2W, DWI, and DCE sequences. The exact combina-

tion of sequences for specific clinical scenarios remains to be defined, but it will certainly rely on the combination with several different sequences to reach the greatest levels of accuracy in cancer detection and characterization [38]. More specifically, based on what has been evaluated to date in studies, current state-of-the-art MRI techniques for prostate

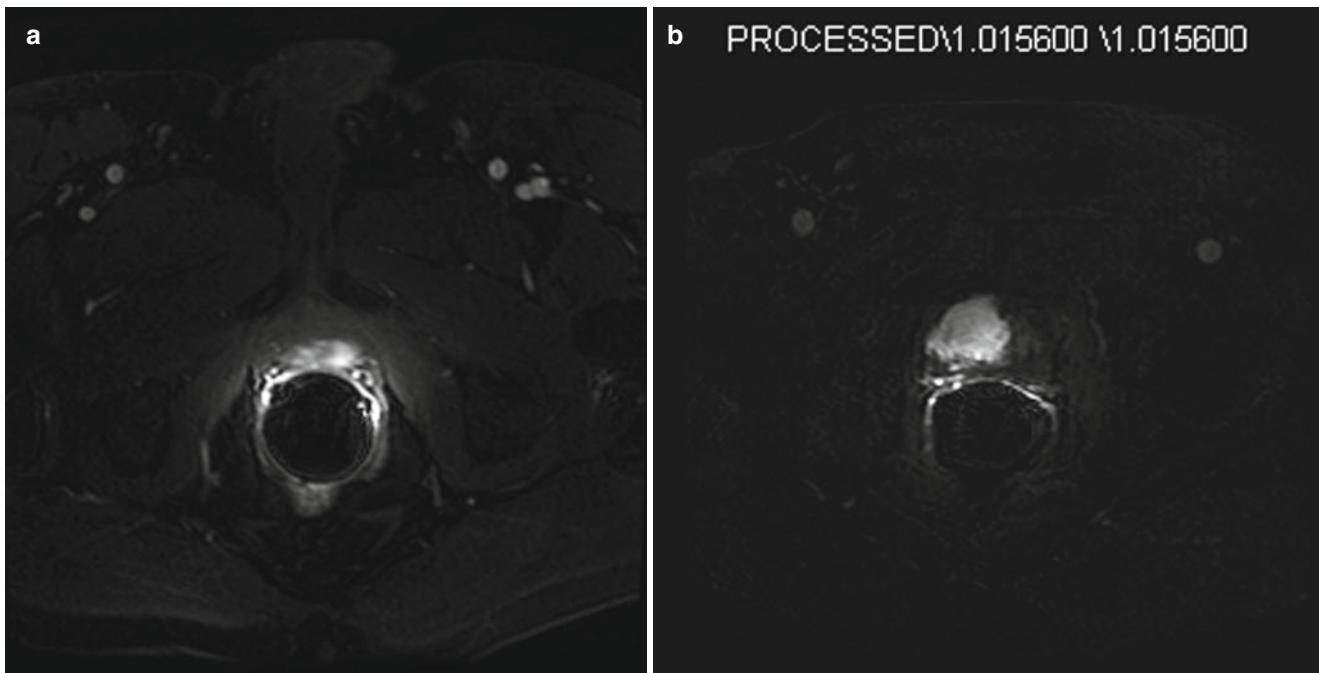


Fig. 56.8 Dynamic contrast enhancement (DCE) MR images. (a) Transverse T1W fat-suppressed image immediately after the injection of intravenous gadolinium. This image shows an arterial enhancing lesion in the left posterior gland. This lesion shows the typical appearance of cancer with early “wash in” of contrast. Note the similar enhancement of the

two femoral arteries at the same time. (b) Subtraction image. Same patient as Figure 56.7. Note matching abnormalities. This image is an arterial phase image with the baseline pre-contrast image subtracted, leaving only the residual arterial contrast as the only signal in the image. Thus the large hyperintense mass on the right represents the arterially enhancing tumor

care are ideally performed on 3 T magnets and are based on the following sequences: T2W fast spin echo in three orthogonal orientations, transverse unenhanced T1W, and dynamic transverse 3D fast spoiled gradient-echo T1W for 90 s after injection of contrast. This data is then processed by specialized software to yield color maps for the DCE series and ADC maps from generated raw DWI. This protocol has been satisfactorily used for the last 5 years for prostate cancer detection, staging, and assessment of radiation therapy at the Brigham and Women’s Hospital (BWH). Moreover, the protocol has been recommended as shown by the consensus reached by 16 European experts at a recent meeting [43]. The overall assessment of stage is based on the determination of whether the tumor is organ confined (T1W/T2W) or beyond the prostate (T3/T4). Seminal vesicle invasion (SVI) and extracapsular extension (ECE) are important factors for staging disease. For SVI, the accepted criteria are low-signal intensity in one or both seminal vesicles (usually high signal in T2W) or disruption or loss of the normal architecture in the ducts or the glands, whereas the criteria for ECE are tumor extension into the periprostatic fat tissue, focal capsular bulge, irregularity, retraction, and rectoprostatic angle obliteration [44]. ECE initially occurs most commonly at the 5 and 7 o’clock locations in the transverse plane.

Wang et al. showed that MRI has better accuracy for predicting SVI than clinical variables. Moreover, the endorectal MRI has shown the most promising results in detecting SVI

with specificity up to 99 % and sensitivity up to 80 % [32]. For assessing ECE, MRI (T2W) has a reported accuracy of between 50 and 90 % [44].

Even though MRI techniques including DCE and MRSI cannot detect precancer lesions, such as prostatic intraepithelial neoplasia, they are good for detecting focal tumor. MRI is also useful for predicting a tumor’s grade. Treatment choice, including active surveillance, relies on MRI to assist in the prediction of a tumor’s behavior; one important aspect of this is the tumor size and prostate gland volume. MRI is known to be better than TRUS for assessing prostate gland volume that is very important for planning and delivering radiation therapy. For instance, patients must be defined as having a prostate smaller than 60 cc for them to be deemed suitable for EBRT or brachytherapy. The criteria for staging prostate carcinoma not only involves defining ECE and SVI but also should concomitantly evaluate pelvic lymph nodes and osseous structures to detect all sites of possible metastases in a single examination [28].

MRI-Guided Prostate Biopsy

Historically, prostate cancer biopsy and local therapies are guided with TRUS. Much of the collective experience with interventional MRI arises from the conventional TRUS techniques, we will review these next.

Conventional TRUS-Guided Prostate Biopsy

TRUS-guided prostate biopsy is by far the most common and frequently used intervention in relation to prostate cancer, given its advantages of relative ease of use, availability, and low cost. It is the initial diagnostic step in the vast majority of cases to obtain tissue samples for pathological evaluation in men suspected of having prostate cancer. TRUS imaging of the prostate has a long history using gray scale and Doppler techniques, even though newer inversion pulsed harmonics and, now in certain select sites, IV microbubble contrast, and ultrasound elastography are under investigation. The basic TRUS imaging used to guide transrectal needle sampling involves a simple visualization of the gland and subdivision of this gland volume into sextants for systematic biopsies. The division allows for 6–12 cores to be removed in an orderly fashion in an attempt to provide uniform gland sampling. Much debate surrounds the recommended approach that ranges from numbers of cores to locations. In general the standard approach is 12 cores with peripheral/lateral aspects of the gland sampled using an 18-gauge (G) side-cutting biopsy needle. The TRUS-guided biopsy procedure is typically performed in an outpatient setting. The patient usually takes prophylactic antibiotics for 1–2 days prior and after the biopsy. Local anesthesia can be used; it is injected into the periprostatic nerves. A technologist can perform TRUS imaging while the urologist acquires the biopsy samples, but more commonly, a single physician does both. Each biopsy sample is labeled, either right or left, and occasionally, more location-specific details are provided. This is, however, very variable and often leads to difficulty in correlating imaging and pathology findings. Each sample is examined separately, and a diagnosis is made between benign, premalignant, prostatic intraepithelia, neoplasia, and adenocarcinoma. In the case of adenocarcinoma, a Gleason score is assigned, depending upon cell types and degrees of differentiation. The percentage tumor volume in each sample is also recorded. The final report also includes the number of positive samples relative to the total samples harvested.

If one critically assesses TRUS image quality, its overall accuracy for detection, characterization, and locoregional staging of prostate cancer then MRI far surpasses TRUS.

Open MRI-Guided Prostate Biopsy

In 1997, the Brigham and Women's Hospital established the first direct transperineal prostate biopsy program using 0.5 T open MRI scanner and validated this approach in over 50 men [45, 46]. To optimize the biopsy yield, the prostate gland is sampled transperineally, thereby maximizing contact with the PZ that is statistically the most likely location of potential cancer and allowing easy access to all parts of the gland, especially the anterior part. This work established a new

approach to prostate biopsies, and many prominent research groups followed suit. The concept was derived from brachytherapy. The needles were introduced freehand using the reference frame of a needle-guidance template commonly used in brachytherapy with grid of holes spaced 5 mm apart. The template was registered to a 0.5 T open MRI scanner using an optical tracking system integrated to the MRI scanner. This registration achieved geometric correlation between the template and patient anatomy, enabling the selection of a hole that will guide a biopsy needle towards the target determined from the MRI scans. By using the template for needle guidance, the needle path was restricted due to the fixed direction of guide holes in the template. In all patients, both targeted and random sampling biopsies were obtained, to allow for the evaluation of the efficacy of targeted sampling and maximizing the diagnostic yield for each patient. To improve needle guidance, navigation software was created by adding specialized modules to 3D Slicer, the powerful open-source visualization and surgical guidance platform [21]. First, target definition and planning functions were added to 3D Slicer. These functions were performed by measuring the coordinates of the suspicious tumors foci and selecting a corresponding hole in the template grid to reach the targets. Target definition was carried out using T2-weighted images after the patient went under general anesthesia. A key feature of the system was volumetric data registration that allows for planning the targets on preoperative high-resolution T2-weighted images mapped onto intraoperative 0.5 T images. With the use of the same volumetric mapping method, patterns like statistical maps or spectroscopic MRI were superimposed on the intraoperative images. Finally, the reconstructed 3D anatomy was blended with all forms of information mentioned above. Due to significant prostate shape changes occurring between preoperative high-field endorectal coil imaging (legs down) and intraoperative 0.5 T imaging (legs up), a deformable registration method based on finite element modeling was developed [47, 48]. The targeting and planning system outlined above also established the tradition of using 3D Slicer as the visualization interface of choice in a long line of experimental image-guided intervention systems.

Efficient and accurate biopsy targeting in the real-time open-MRI environment demanded methods for needle tracking. Needles are visible in MRI due to their susceptibility artifact. Paramagnetic needles when imaged produce field distortions that appear as local regions of signal loss and, in some cases, signal enhancement [49]. The size and location of the artifact change with the material properties of the needle, imaging signal, image resolution, and the relative orientation of the needle, B₀ field and the gradient field. In other words, the needle is usually not where it appears to be in the MR image. There is a compromise between imaging speed and quality that impacts needle localization, accuracy, and reliability [50]. The susceptibility artifacts produced by needles in magnets of various field strengths were

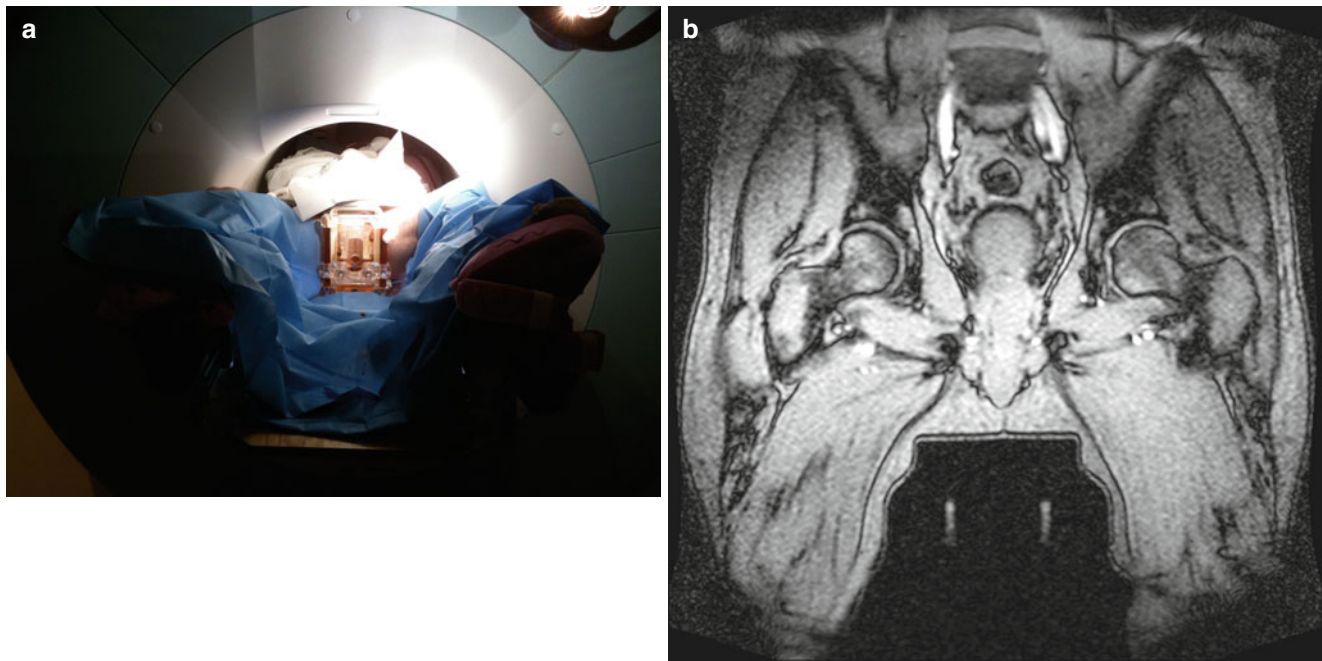


Fig. 56.9 (a) Pre-transperineal prostate biopsy setup. (b) This coronal gradient-echo image shows the patient in the pre-biopsy setup position with the transperineal template guide positioned between his legs. Two

linear stripes of signal from the Z-frame are seen below the template. The Z-frame allows registration of the template and patients prostate gland

characterized. Techniques have been proposed for optimizing the visualization of image artifacts and driving the scan plane [51]. Recent work reported on the feasibility of mapping the spatial displacement of the needle susceptibility artifact versus the true needle position [52, 53].

A detailed investigation of needle placement accuracy study concluded that precise and accurate placement of needle may be best achieved by robotic needle placement [54].

New 3 T magnet bore size at 70 cm diameter now allow us to perform transperineal 3T MR-guided prostate biopsy. We at Brigham and Women's Hospital (BWH) now perform this regularly at 3 T, with the patient in prone position, under intravenous conscious sedation (IVCS) (Figs. 56.9 and 56.10). The perineal template is used and manual needle insertion is performed under MR guidance (Figs. 56.6 and 56.9). We obtain a full multiparametric MR exam several days to weeks prior to the biopsy procedure. These images are used to define targets for sampling. The images are imported into 3D Slicer (Fig. 56.11) and registered to the procedure images with Z-frame, using the method introduced by Fichtinger et al. [18]. This approach provides the unique opportunity to obtain site-specific pathological samples from image abnormalities.

MR Guided Focal Therapy

This unique ability to validate the MR findings along with the improvements of MR for detection and characterization of focal disease allows for investigation of image-guided

focal therapy. Many centers are using the MR and US capabilities to guide High Intensity Focused Ultrasound (HIFU), cryotherapy, laser or photodynamic therapy. We have completed preclinical trials in MR-guided FUS surgery (Fig. 56.12a, b) and demonstrated our ability to induce focal prostate necrosis. The exciting feature of this approach to focal therapy is the ability to closely monitor the temperature change in near real-time with MR thermometry (Fig. 56.2b). This allows for accurate placement of sonications and immediate feedback of therapeutic result. New clinical trials are underway which will allow carefully assessment of this exciting new approach to focal therapy for prostate cancer have begun and are underway.

MRI-Assisted Prostate Biopsy with Real-Time TRUS Guidance

To marry the convenience of TRUS with the superior anatomical visualization of MRI in prostate biopsy, fusion of preoperative high-resolution MRI and intraoperative real-time TRUS has been proposed [55–57]. This method critically depends on the assumption of spatially correct co-registration between intraoperative decubitus ultrasound and pre-procedural supine MRI in the presence of extreme tissue motion and deformation, a problem that, at the moment, does not have a clinically robust solution. A sufficiently accurate and robust solution will undoubtedly turn up, but this approach will always suffer from the lack of direct and immediate pathological evidence of whether the

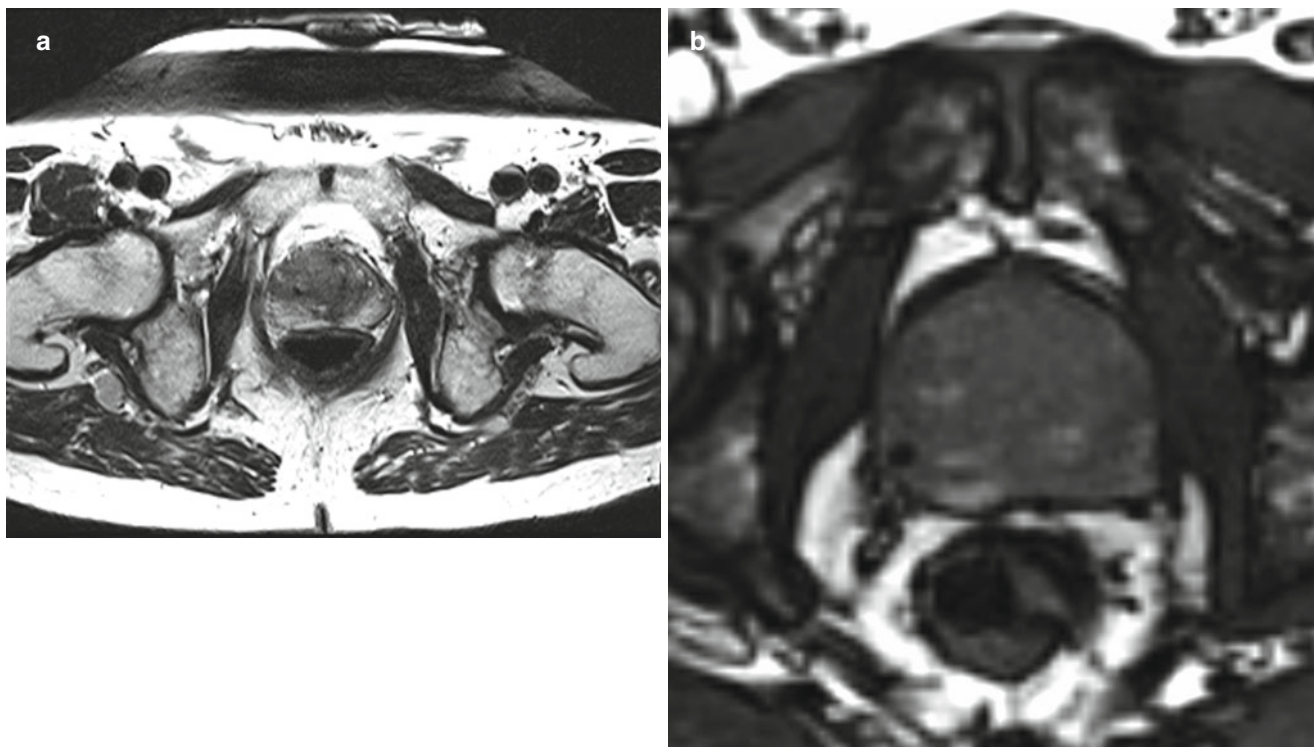


Fig. 56.10 MR-guided prostate biopsy needle in place. (a) This is an transverse T2W image with a biopsy needle in place—see small black void in 9 o'clock position in the right mid-gland. (b) This transverse

gradient-echo image “near real time” shows a needle in position in the right side of the prostate. Note the focal black-signal void. This is more conspicuous than in (a) but lacks the T2W contrast inside the prostate

registration was indeed correct and the biopsy was executed as planned in MRI. In contrast to the image fusion-based approach, in situ MRI-guided biopsy eliminates spatial uncertainty and doubt from the procedure.

Robotically Assisted MRI-Guided Prostate Biopsy

Although the use of MR imaging in prostate cancer biopsy and therapy guidance is highly desirable, physical limitations of conventional closed MRI scanners present significant obstacles. Robotic assistance is the only viable option to execute needle placement inside the long cylindrical bore of conventional MRI scanners. Compounding the challenges further, the strong magnetic field excludes the use of most metals, electronics, and electrodynamic actuation. Despite or perhaps owing to these challenges, MRI-guided prostate cancer interventions have been a subject of intense research. The prostate has appeared to be a kind of anatomical target that is accessible for minimally invasive needle-based interventions through either the skin or a body cavity particularly when there is a well-defined boundary; the prostate is not entirely rigid but also not exceedingly soft and when the prostate is not entirely stationary but also not prohibitively mobile. In short, coincident demand from the clinical side and supply from engineering side propelled

medical robotics to be the subject of recent activities in needle-based prostate cancer interventions. Thus far, however, very little of those works have reached clinical patient trials, owing to the formidable difficulties that we will review shortly.

Technical Challenges Arising from MRI

In addition to previously mentioned challenges, MRI-guided robotic biopsy involves more difficulties, each of which we will elaborate on next.

Accuracy

Prostate cancer is a progressive disease, the malignant potential of which increases with tumor volume. A 0.5 cc prostate cancer volume has been proposed as the limit of clinically significant prostate cancer foci, which is a volume that corresponds to a tumor sphere with a diameter of 9.8 mm. An MRI-guided biopsy system employing a targeting accuracy of 5 mm or better could reliably sample clinically significant prostate cancer foci. Although it may seem like a lenient requirement, it has been notoriously difficult to meet in a consistent and reliable manner in clinical trials, which explains why there have been just a very few MRI-guided robotic intervention systems ever used on actual patients.

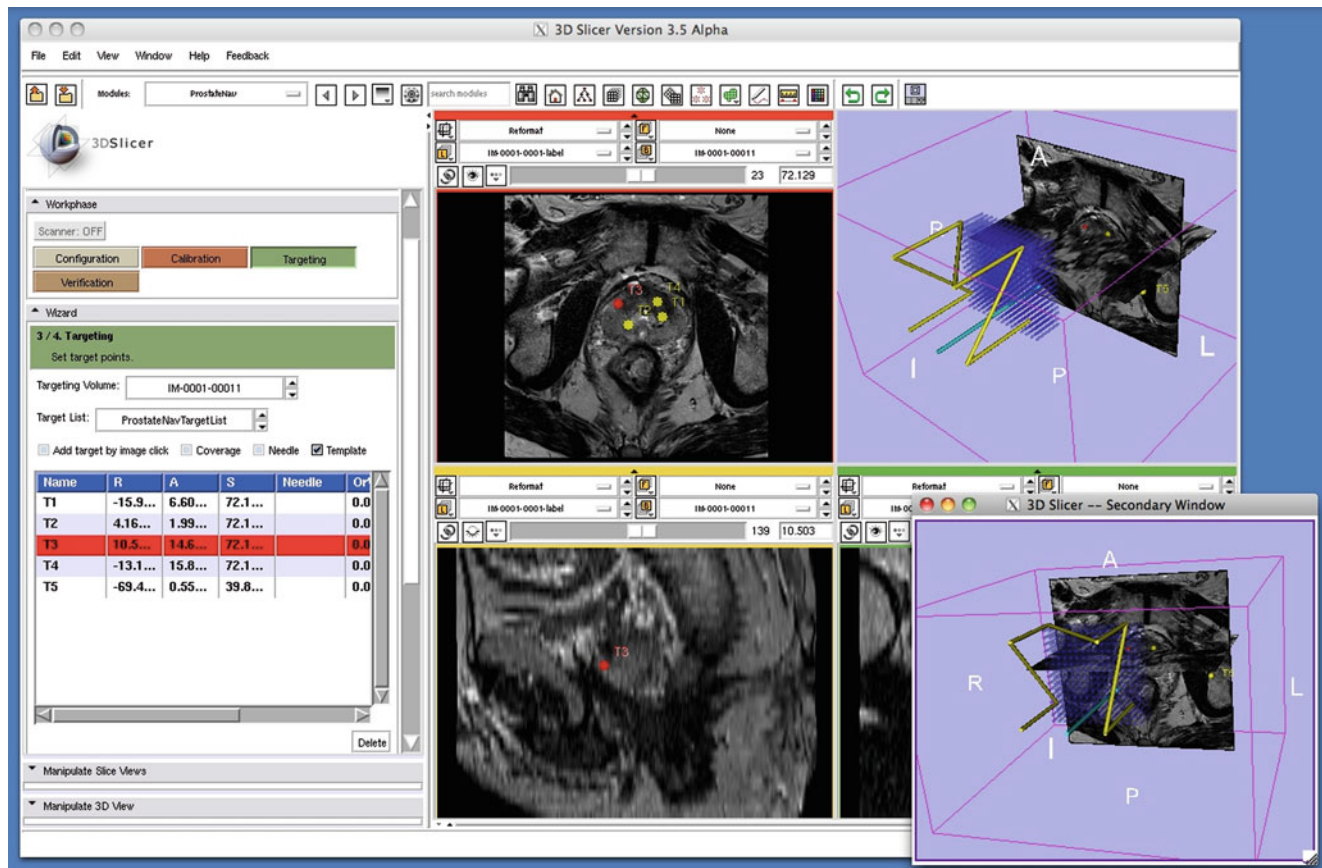


Fig. 56.11 3D Slicer prostate module. This single screen shot from the prostate biopsy module in 3D Slicer (www.slicer.org) shows four images: *top left*, transverse T2W image with pre-defined biopsy targets;

top right, the Z frame and all template holes registered to the T2W image; *bottom left*, a sagittal image showing a target location; and *bottom right*, Z-frame and template again in alternative orientation

Workspace

To have a direct access to the patient during imaging inside the long and narrow scanner bore, compactness is a major requirement. The end effector, the part that makes contact with the patient, is usually designed to be small and slender, while the actuation, power, and control mechanisms may be larger as they can be situated outside the bore.

MR Compatibility

For a system to be considered MRI compatible, it must meet three requirements: (1) safety in the MRI environment, (2) preservation of image quality, and (3) an ability to operate unaffected by the scanner's electric and magnetic fields [58]. Ferromagnetic materials must be avoided entirely because they cause image artifacts and distortion due to field inhomogeneities, and they pose a dangerous projectile risk. Non-ferromagnetic metals such as aluminum, brass, titanium, high strength plastic, and composite materials are permissible. However, the use of any conductive materials in the vicinity of the scanner's isocenter must be limited because of the potential for induced eddy currents to locally deform the magnetic field homogeneity. Electrical systems must be properly shielded and filtered and designed to limit noise emissions. Care must also be

taken to avoid resonance and heating. Reviews of MRI-compatible robotic systems to date for image-guided interventions were presented in [59, 60].

Registration Between Robot and MRI

The development of MRI-guided robotic intervention instruments is complicated by the need to track in real-time the pose (i.e., position and orientation) of these instruments within the MRI scanner. This, seemingly innocuous issue, is also a notoriously difficult problem to solve in the operating room and has great impact on every aspect of the system, including its accuracy and ease of use. Several approaches have been tried out in MRI-guided robots and passive devices.

Joint Encoder Tracking

Here the device's pose is determined by joint encoders at the articulated joints [58–62], while the device is precisely calibrated with respect to the scanner coordinate system, and it is rigidly secured to the scanner's table.

Passive MRI Fiducial Tracking

Here the device's pose is determined by localizing passive fiducial markers embedded within the device. For guiding

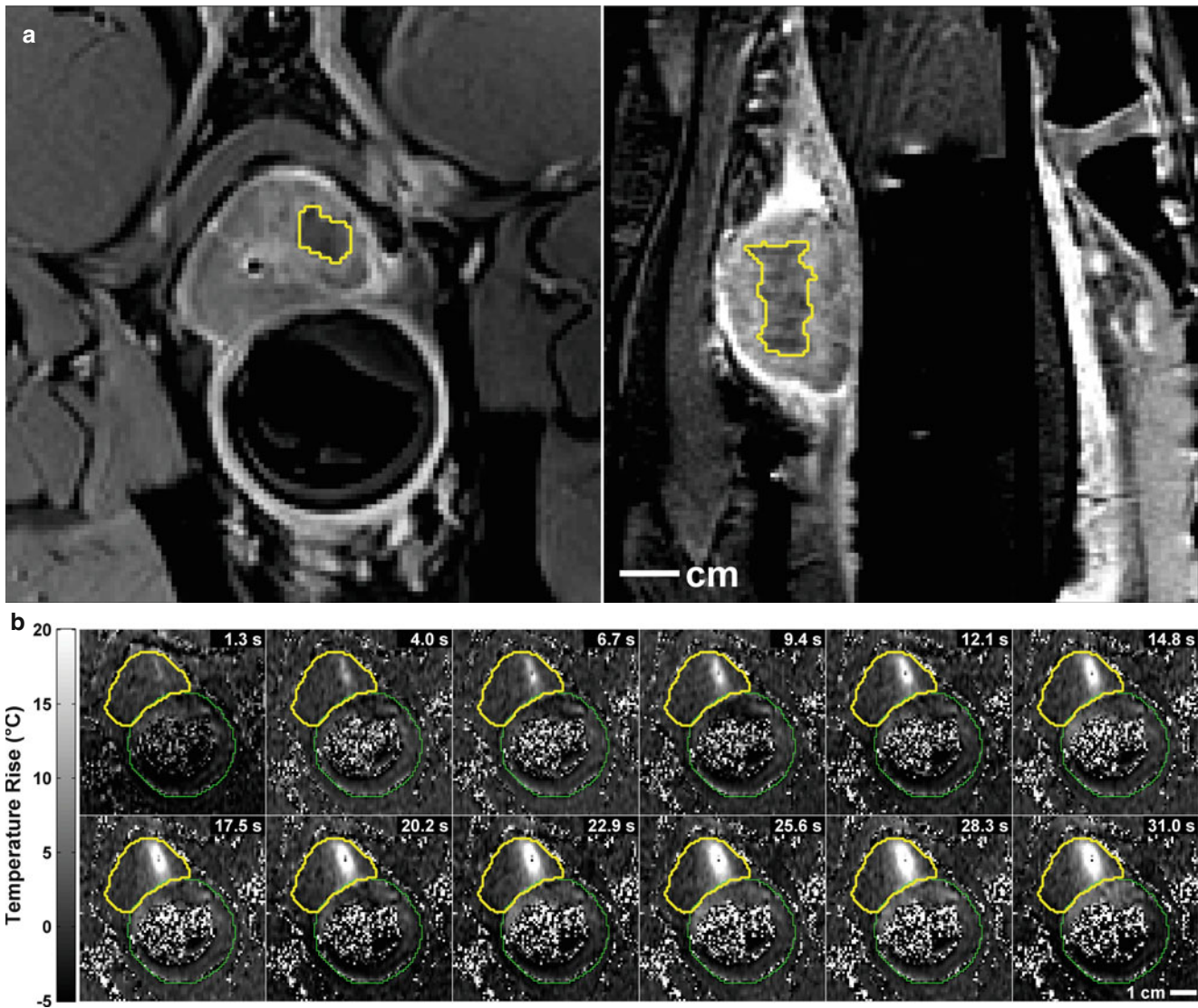


Fig. 56.12 (a) Two images obtained after MR-guided focused ultrasound surgery (FUS) to a small region of the prostate in a preclinical trial. The images show the well-defined non-perfused region after the IV gadolinium. (b) Multiple MR thermometry images, from time 1.3–

31.0 s, acquired during the delivery of FUS energy show the local heating (white area) within the prostate. Thus local heat delivered can be monitored in real-time during the procedure

transperineal needles, Susil et al. used a brachytherapy template in which the holes were filled with contrast material preoperatively localized in standard T1- or T2-weighted images and then registered to scanner coordinates [23]. In a transrectal biopsy device, Beyersdorff et al. used a gadolinium-filled fiducial marker sleeve coaxial with the biopsy needle [14].

Optical Pose Tracking

Here the device's pose is determined by an optical tracking system calibrated to the scanner coordinate system [51], an approach that requires line of sight between the optical tracking cameras and the device, and it also requires passive optical targets or tethered light-emitting diodes to be attached to the end effector of the robot.

Gradient Field Sensing

Here the device's pose is determined by a tethered 3-axis magnetic sensor embedded within the device that senses the scanner gradient fields. Hushek et al. investigated a commercial tracking mechanism called EndoScout (Robin Medical Systems, Baltimore, MD) that is approved for use in an open MRI scanner by the Food and Drug Administration (FDA) [63]. In present implementations, the tracking sensors must be placed close to the MRI magnet's isocenter and thus may occupy critical workspace. This approach also requires a precise one-time calibration procedure to be performed over the entire field of interest in each MRI system on which it is installed.

Micro-Tracking Coils

Here the device's pose is determined by three or more tethered micro-tracking coils that are embedded within the device

to sense custom-programmed MRI pulse sequences. Micro-tracking coils, originally reported in [64], were employed by Krieger et al. to provide exquisitely accurate (0.2 mm) full 6 degree of freedom (DOF) tracking at 20 Hz [65]. Its disadvantages are lack of robustness due to the delicate micro-coils, the need for three (or more) dedicated scanner channels, and need for custom-programmed tracking sequences that are not standard on commercial MRI scanners. Presently, the need for custom-programmed tracking sequences renders this approach impractical for widespread clinical deployment.

Hybrid Tracking

This approach determines the pose of the intervention device by combining a one-time initial passive fiducial tracking with MRI-compatible joint encoding to provide full 6-DOF instrument tracking throughout an MRI-guided interventional procedure [62].

Target Motion

As MRI scanning is a rather slow process, there is an ample chance for the prostate to move between imaging and needle placements. During transrectal needle placement, since the access route is slow and the action of the needle is fast, the target tends to dislocate less significantly. The feasibility of using MRI as an alternative tool for surgical navigation in prostate biopsy was studied by Hata et al. [21]. Through patient trials, they proved that T2-weighted interventional MR imaging with 3D visualization software can be used to guide needle placement in prostate biopsies. For MRI-guided target tracking, radio-frequency (RF) signal-based and image-based methods have been proposed. In RF signal-based tracking, the subject is scanned using a custom-designed imaging sequence before and after motion. Translational motion information is then computationally derived from the resulting echo of the RF coil. Hata et al. developed an intraoperative MRI registration algorithm using projection profile matching of the RF echo [66]. The main drawbacks of this technique are lack of 3D positional information and, more importantly, the requirement of access to the control sequence of the MRI scanner that is only available through confidential research agreement with the manufacturer. A clinically practical solution to the prohibitively long volume acquisition and registration times and unavailability of custom scanning sequences is to acquire multiple statically set slices at the scanner's isocenter and register those with the MRI volume used for target planning [67].

Access Approaches for MRI-Guided Robotic Prostate Biopsy Systems

Transrectal Approach

Transrectal access is excellently tolerated by patients; it requires only local anesthesia and practitioners usually have

extensive prior experience in transrectal biopsy with ultrasound guidance. In exploring the transrectal access with MRI guidance, Beyersdorff et al. used a transrectal needle guide in 1.5 T magnets with surface imaging coils with a prone patient position [14]. Engelhard et al. used a similar setup with a supine patient position [17].

Krieger et al. at the Johns Hopkins Hospital developed the first actuated transrectal prostate biopsy device for use inside the bore of closed high-field MRI scanners and named the device access to prostate tissue (APT-MRI) where APT stands for "Access to Prostate" [65]. The patient was positioned in a prone position with the pelvis slightly elevated. The APT-MRI provided independent rotation and translation of the needle guide inside the rectum and insertion of a curved biopsy or fiducial marker implant needle through the rectum into the prostate. The end effector also housed a single-loop imaging coil that was mechanically decoupled from all moving parts of the device, thus providing high-quality MR images of the target. The APT-MRI featured three tethered micro-tracking coils that are embedded within the device to sense custom-programmed MRI pulse sequences. The micro-tracking coils provided 6-DOF spatial registration at 0.2 mm accuracy and 20 Hz frequency between the device and the MRI scanner's coordinate system. The high tracking update rate, accurate localization, and slow speed of the device made it possible for the physician to manually power the actuation cables. In effect, the physician used visual servo control to navigate the needle onto a target that was then advanced from outside the bore. Owing to these design features, the APT-MRI was progressed from idea to clinical trials in less than 2 years. The APT-MRI supported a variety of clinical trials to date in prostate biopsies and fiducial marker insertion [68–70]. The main disadvantages of the APT-MRI were its need for four dedicated MRI scanner channels and for custom-programmed tracking sequences that are not standard on commercial MRI scanners.

To make the APT-MRI portable between average MRI scanners, Krieger et al. modified the system by replacing the micro-tracking coils with hybrid tracking using a combination of passive fiducials and joint encoders [62]. Initially the robot's pose was determined by localizing passive fiducial markers embedded within the device. After an initial pose was determined with passive markers, electro-optical joint encoders provided the relative position of the device. Krieger et al. also replaced the custom-made curved needles with standard MRI-compatible biopsy needles, and they detached the actuation cables. The resulting system, shown in Fig. 56.13a, was tested in patient trials at different clinical sites [62]. It is of note that the associated targeting interface, shown in Fig. 56.13b, is based on the 3D Slicer (www.slicer.org) open-source medical image visualization and analysis platform.

Transperineal Approach

When the number of needle insertions is greater, such as in brachytherapy implants, the transperineal approach is preferred

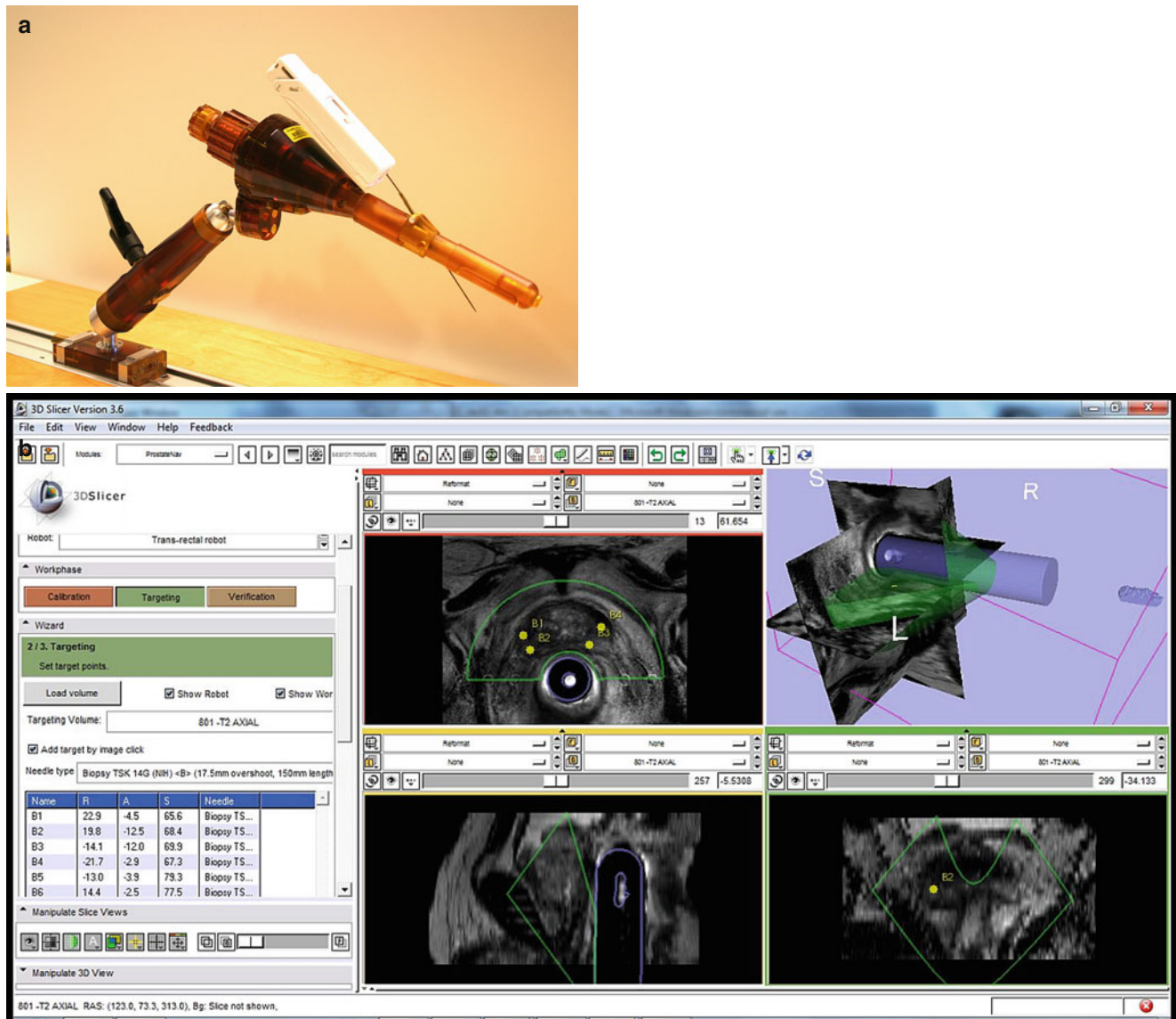


Fig. 56.13 The APT-MRI transrectal prostate biopsy system developed at the Johns Hopkins University by Krieger et al. [62]. (a) The fully MRI-compatible manually actuated 3-DOF device supports conventional MRI-compatible biopsy needles. (b) The biopsy target plan-

ning and monitoring program is based on the 3D Slicer open-source medical image visualization and analysis platform (www.slicer.org). The image is courtesy of Dr. Andras Lasso (Queen's University, Canada)

over the transrectal, to avoid excessive physical damage to the anterior rectal wall. Patients with large prostates (>50 cc) may be excluded from transperineal procedures due to pubic arch interference. This problem, however, has become less of an issue nowadays as practitioners are more skilled and as hormone therapy is used to reduce the volume of the gland prior to intervention [71]. Transperineal procedures are typically performed with lumbar or full anesthesia and some also advocate local anesthesia [71]. As prostate cancer tends to occur in the PZ, transperineal needles have a higher likelihood of encountering cancer than transrectal needles. Transperineal needles also require fewer needle sticks to systematically sample the gland. At the same time, transperineal needles may bend and deflect in multiple layers of inhomogeneous tissue.

As mentioned earlier, MRI-guided transperineal prostate intervention was first demonstrated at the Brigham and Women's Hospital (BWH) with open MRI scanners [45, 46]. The BWH group went on to use the MRI-compatible robot reported in [58] by adapting it to the transperineal needle placement demonstrated in phantom studies [51]. Here, the pose of the robot was determined by an optical tracking system previously calibrated to the scanner coordinate system. When open MRI scanners were discontinued, research on high-field closed MRI scanners intensified. Susil et al. used conventional closed MRI scanners. For needle guidance, they applied a brachytherapy template in which the holes were filled with contrast material preoperatively localized in standard T1- or T2-weighted images and then registered to scanner

coordinates [23]. The BWH and the Johns Hopkins University groups jointly developed a pneumatically actuated transperineal intervention robot and evaluated it in phantom and patient compatibility trials [54, 72, 73]. Tadakuma et al. reported *ex vivo* studies of a dielectric elastomer-actuated MRI-compatible robot [74]. Stoianovici et al. reported phantom studies of a pneumatic robot [75]. Goldenberg et al. reported phantom studies with a piezo-actuated robotic actuation [76]. Though each of these works showed innovative technical solutions, they have not been used clinically.

The first transperineal MRI-guided robotic system ever used clinically on patients was developed by Van den Bosch et al., who reported patient studies in marker seed placement with a hydraulic/pneumatic robot [77]. This device was manually translated and rotated, resulting in five DOF. The salient feature of this device is a pneumatically driven tapping device to insert a needle stepwise into the prostate using a controller unit outside the scanning room. The target and entry points were defined in high-resolution 3D-balanced steady-state-free precession (bSSFP) scan made possible through a T2/T1-weighted contrast. During the needle insertion, fast 2D bSSFP images were generated to track the needle online and reported, compared to conventional needle insertion, high needle placement accuracy and significant reduction in prostate deformation and needle deflection.

Transgluteal Approach

As this approach is significantly more invasive than the transrectal and transperineal routes, it should be reserved for patients with prior history of rectal or genitourinary surgery. Zangos et al. reported results from 19 patients in prostate biopsy, with transgluteal access on a 1.5 T closed-bore scanner, using the Innomotion pneumatic MRI-compatible robot (Innomedic GmbH, Philippsburg-Rheinsheim, Germany) [78]. The robot was registered to the MRI scanner with gadolinium-filled passive fiducial markers attached to the needle guide. They used body surface coils and T1-weighted gradient-echo fast low-angle shot and T2-weighted true-fast imaging with steady-state precession sequences for target planning. The targeting software of the system calculated the trajectory and then moved the guiding arm to the insertion point. An MRI-compatible cannula was advanced manually, and biopsies were performed with the coaxial technique by using a 15-gauge pencil tip needle. The Innomotion robot is a generic multipurpose device to support MRI-guided needle placement. Although the kinematic design of the device is not suited for transrectal or transperineal access, it served transgluteal access excellently. Unfortunately, as the Innomotion device does not have a needle driver, the patient needed to be moved out of the scanner after imaging for needle insertion. They recorded an impressive median intervention time of 39 min for sextant biopsy and did not observe procedure-related complications.

Concluding Remarks

Clearly, MRI has a great potential role in increasing specificity of screening for early prostate cancer and in the targeting of biopsy sites to avoid unnecessary biopsies and predict the outcome of biopsies. In addition to detection of prostate cancer, accurate staging of the disease is also essential for making decisions on therapy options. Robotic assistance appears to be a useful adjunct to MRI in that it allows for the performing of the biopsy and interventions inside the bore under direct MRI guidance. Although robotic assistant systems may not emerge as part of the standard care in the future, they presently have an essential role in MRI imaging research. In the future we believe that MR imaging will become an established component of active surveillance protocols. It will also play an increasing role in treatment guidance, especially with subtotal gland or focal therapies.

Altogether, MRI has undoubtedly a bright and long future in prostate cancer imaging and intervention, but continued clinical research still remains to be done until MRI is well established as part of routine clinical care.

References

1. Andriole GL, Crawford ED, Grubb 3rd RL, Buys SS, Chia D, Church TR, et al. Prostate cancer screening in the randomized prostate, lung, colorectal, and ovarian cancer screening trial: mortality results after 13 years of follow-up. *J Natl Cancer Inst.* 2012;104(2):125–32.
2. Schröder FH, Hugosson J, Roobol MJ, Tammela TL, Ciatto S, Nelen V, et al. Screening and prostate-cancer mortality in a randomized European study. *N Engl J Med.* 2009;360(13):1320–8.
3. The American Cancer Society (ACS) Website. Available at: <http://www.cancer.org/Cancer/ProstateCancer/DetailedGuide/prostate-cancer-key-statistics>. Accessed 7 June 2012.
4. Barbiere JM, Greenberg DC, Wright KA, Brown CH, Palmer C, Neal DE, Lyratzopoulos G. The association of diagnosis in the private or NHS sector on prostate cancer stage and treatment. *J Public Health (Oxf).* 2012;34(1):108–14.
5. Norberg M, Egevad L, Holmberg L, Sparen P, Norlen BJ, Busch C. The sextant protocol for ultrasound-guided core biopsies of the prostate underestimates the presence of cancer. *Urology.* 1997;50(4):562–6.
6. Rabbani F, Stroumbakis N, Kava BR, Cookson MS, Fair WR. Incidence and clinical significance of false-negative sextant biopsies of the prostate. *Urologie A.* 1998;37(6):660.
7. Roehl KA, Antenor JA, Catalona WJ. Robustness of free prostate specific antigen measurements to reduce unnecessary biopsies in the 2.6 To 4.0 ng/ml range. *J Urol.* 2002;168(3):922–5.
8. Terris MK, Wallen EM, Stamey TA. Comparison of mid-lobe versus lateral systematic sextant biopsies in the detection of prostate cancer. *Urol Int.* 1997;59(4):239–42.
9. Wefer AE, Hricak H, Vigneron DB, Coakley FV, Lu Y, Wefer J, et al. Sextant localization of prostate cancer: comparison of sextant biopsy, magnetic resonance imaging and magnetic resonance spectroscopic imaging with step section histology. *J Urol.* 2000;164(2):400–4.
10. Halpern EJ, Ramey JR, Strup SE, Frauscher F, McCue P, Gomella LG. Detection of prostate carcinoma with contrast-enhanced sonography using intermittent harmonic imaging. *Cancer.* 2005;104(11):2373–83.

11. Kelloff GJ, Choyke P, Coffey DS. Challenges in clinical prostate cancer: role of imaging. *AJR Am J Roentgenol.* 2009;192(6):1455–70.
12. Mitterberger M, Pinggera GM, Horninger W, Bartsch G, Strasser H, Schafer G, et al. Comparison of contrast enhanced color Doppler targeted biopsy to conventional systematic biopsy: impact on Gleason score. *J Urol.* 2007;178(2):464–8; discussion 468.
13. Anastasiadis AG, Lichy MP, Nagele U, Kuczyk MA, Merseburger AS, Hennenlotter J, et al. MRI-guided biopsy of the prostate increases diagnostic performance in men with elevated or increasing PSA levels after previous negative TRUS biopsies. *Eur Urol.* 2006;50(4):738–48; discussion 748–9.
14. Beyersdorff D, Winkel A, Hamm B, Lenk S, Loening SA, Taupitz M. MR imaging guided prostate biopsy with a closed MR unit at 1.5 T: initial results. *Radiology.* 2005;234(2):576–81.
15. D'Amico A, Cormack R, Kumar S, Tempny CM. Real-time magnetic resonance imaging-guided brachytherapy in the treatment of selected patients with clinically localized prostate cancer. *J Endourol.* 2000;14(4):367–70.
16. D'Amico AV, Cormack RA, Tempny CM. MRI-guided diagnosis and treatment of prostate cancer. *N Engl J Med.* 2001;344(10):776–7.
17. Engelhard K, Hollenbach HP, Kiefer B, Winkel A, Goeb K, Engehausen D. Prostate biopsy in the supine position in a standard 1.5-T scanner under real time MR imaging control using a MR-compatible endorectal biopsy device. *Eur Radiol.* 2006;16(6):1237–43.
18. Fichtinger G, DeWeese TL, Patriciu A, Tanacs A, Mazilu D, Anderson JH, et al. System for robotically assisted prostate biopsy and therapy with intraoperative CT guidance. *Acad Radiol.* 2002;9(1):60–74.
19. Hambrock T, Futterer JJ, Huisman HJ, Hulsbergen-van de Kaa C, van Basten JP, van Oort I, et al. Thirty-two-channel coil 3T magnetic resonance-guided biopsies of prostate tumor suspicious regions identified on multimodality 3T magnetic resonance imaging: technique and feasibility. *Invest Radiol.* 2008;43(10):686–94.
20. Hambrock T, Somford DM, Hoeks C, Bouwense SA, Huisman H, Yakar D, et al. Magnetic resonance imaging guided prostate biopsy in men with repeat negative biopsies and increased prostate specific antigen. *J Urol.* 2010;183(2):520–7.
21. Hata N, Jinzaki M, Kacher D, Cormack R, Gering D, Nabavi A, Silverman SG, D'Amico AV, Kikinis R, Jolesz FA, Tempny CM. MR imaging-guided prostate biopsy with surgical navigation software: device validation and feasibility. *Radiology.* 2001;220(1):263–8.
22. Pondman KM, Futterer JJ, ten Haken B, Schultze Kool LJ, Witjes JA, Hambrock T, Macura KJ, Barentsz JO. MR-guided biopsy of the prostate: an overview of techniques and a systematic review. *Eur Urol.* 2008;54(3):517–27.
23. Susil RC, Camphausen K, Choyke P, McVeigh ER, Gustafson GS, Ning H, Miller RW, Atalar E, Coleman CN, Menard C. System for prostate brachytherapy and biopsy in a standard 1.5 T MRI scanner. *Magn Reson Med.* 2004;52(3):683–7.
24. Susil RC, Menard C, Krieger A, Coleman JA, Camphausen K, Choyke P, Fichtinger G, Whitcomb LL, Coleman CN, Atalar E. Transrectal prostate biopsy and fiducial marker placement in a standard 1.5T magnetic resonance imaging scanner. *J Urol.* 2006;175(1):113–20.
25. Tempny C, Straus S, Hata N, Haker S. MR-guided prostate interventions. *J Magn Reson Imaging.* 2008;27(2):356–67.
26. Zangos S, Eichler K, Engelmann K, Ahmed M, Dettmer S, Herzog C, Pegios W, Wetter A, Lehnert T, Mack MG, Vogl TJ. MR-guided transgluteal biopsies with an open low-field system in patients with clinically suspected prostate cancer: technique and preliminary results. *Eur Radiol.* 2005;15(1):174–82.
27. Klotz L, Thompson I. Early prostate cancer – treat or watch? *N Engl J Med.* 2011;365(6):569.
28. Hricak H, Choyke PL, Eberhardt SC, Leibel SA, Scardino PT. Imaging prostate cancer: a multidisciplinary perspective. *Radiology.* 2007;243:28–53.
29. Langer DL, van der Kwast TH, Evans AJ, Plotkin A, Trachtenberg J, Wilson BC. Prostate tissue composition and MR measurements: investigating the relationships between ADC, T2, K(trans), v(e), and corresponding histologic features. *Radiology.* 2010;255:485–94.
30. Oto A, Kayhan A, Jiang Y, Tretiakova M, Yang C, Antic T. Prostate cancer: differentiation of central gland cancer from benign prostatic hyperplasia by using diffusion-weighted and dynamic contrast-enhanced MR imaging. *Radiology.* 2010;257:715–23.
31. Arumainayagam N, Kumaar S, Ahmed HU, Moore CM, Payne H, Freeman A. Accuracy of multiparametric magnetic resonance imaging in detecting recurrent prostate cancer after radiotherapy. *BJU Int.* 2010;106:991–7.
32. Wang L, Hricak H, Kattan MW, Chen HN, Kuroiwa K, Eisenberg HF. Prediction of seminal vesicle invasion in prostate cancer: incremental value of adding endorectal MR imaging to the Kattan nomogram. *Radiology.* 2007;242:182–8.
33. Yoshimitsu K, Kiyoshima K, Irie H, Tajima T, Asayama Y, Hirakawa M, Ishigami K, Naito S, Honda H. Usefulness of apparent diffusion coefficient map in diagnosing prostate carcinoma: correlation with stepwise histopathology. *J Magn Reson Imaging.* 2008;27:132–9.
34. Zelfhof B, Pickles M, Liney G, Gibbs P, Rodrigues G, Kraus S, Turnbull L. Correlation of diffusion-weighted magnetic resonance data with cellularity in prostate cancer. *BJU Int.* 2009;103:883–8.
35. Woodfield CA, Tung GA, Grand DJ, Pezzullo JA, Machan JT, Renzulli 2nd JF. Diffusion-weighted MRI of peripheral zone prostate cancer: comparison of tumor apparent diffusion coefficient with Gleason score and percentage of tumor on core biopsy. *AJR Am J Roentgenol.* 2010;194:W316–22.
36. Gibbs P, Liney GP, Pickles MD, Zelfhof B, Rodrigues G, Turnbull LW. Correlation of ADC and T2 measurements with cell density in prostate cancer at 3.0 Tesla. *Invest Radiol.* 2009;44:572–6.
37. Ito Y, Nakanishi K, Narumi Y, Nishizawa Y, Tsukuma H. Clinical utility of apparent diffusion coefficient (ADC) values in patients with prostate cancer: can ADC values contribute to assess the aggressiveness of prostate cancer? *J Magn Reson Imaging.* 2011;33:167–72.
38. Turkbey B, Pinto PA, Mani H, Bernardo M, Pang Y, McKinney YL. Prostate cancer: value of multiparametric MR imaging at 3 T for detection-histopathologic correlation. *Radiology.* 2010;255:89–99.
39. Turkbey B, Shah VP, Pang Y, Bernardo M, Xu S, Kruecker J. Is apparent diffusion coefficient associated with clinical risk scores for prostate cancers that are visible on 3-T MR images? *Radiology.* 2011;258:488–95.
40. Mullerad M, Hricak H, Kuroiwa K, Pucar D, Chen HN, Kattan MW. Comparison of endorectal magnetic resonance imaging, guided prostate biopsy and digital rectal examination in the preoperative anatomical localization of prostate cancer. *J Urol.* 2005;174:2158–63.
41. Kumar V, Jagannathan NR, Kumar R, Nayyar R, Thulker S, Gupta SD, et al. Potential of 1H MR spectroscopic imaging to segregate patients who are likely to show malignancy of the peripheral zone of the prostate on biopsy. *J Magn Reson Imaging.* 2009;30(4):842–8.
42. Weinreb JC, Blume JD, Coakley FV, Wheeler TM, Cormack JB, Sotito CK. Prostate cancer: sextant localization at MR imaging and MR spectroscopic imaging before prostatectomy—results of ACRIN prospective multi-institutional clinicopathologic study. *Radiology.* 2009;251:122–33.
43. Dickinson L, Ahmed HU, Allen C, Barentsz JO, Carey B, Futterer JJ, et al. Magnetic resonance imaging for the detection,

- localisation, and characterisation of prostate cancer: recommendations from a European consensus meeting. *Eur Urol.* 2011;59(4):477–94.
44. Futterer JJ. MR imaging in local staging of prostate cancer. *Eur J Radiol.* 2007;63:328–34.
 45. Cormack RA, D'Amico AV, Hata N, Silverman S, Weinstein M, Tempany CM. Feasibility of transperineal prostate biopsy under interventional magnetic resonance guidance. *Urology.* 2000;56:663–4.
 46. D'Amico AV, Tempany CM, Cormack R, Hata N, Jinzaki M, Tuncali K, et al. Transperineal magnetic resonance image guided prostate biopsy. *J Urol.* 2000;164:385–7.
 47. Hirose M, Bharatha A, Hata N, Zou KH, Warfield SK, Cormack RA, et al. Quantitative MRI imaging assessment of prostate gland deformation before and during MRI imaging-guided brachytherapy. *Acad Radiol.* 2002;9(8):906–12.
 48. Bharatha A, Hirose M, Hata N, Warfield SK, Ferrant M, Zou KH, et al. Evaluation of three-dimensional finite element-based deformable registration of pre- and intraoperative prostate imaging. *Med Phys.* 2001;28:2551–60.
 49. Seppenwoolde JH, Vieregger MA, Bakker CJ. Passive tracking exploiting local signal conservation: the white marker phenomenon. *Magn Reson Med.* 2003;50(4):784–90.
 50. van der Weide R, Bakker CJ, Vieregger MA. Localization of intravascular devices with paramagnetic markers in MR images. *IEEE Trans Med Imaging.* 2001;20(10):1061–71.
 51. DiMaio SP, Pieper S, Chinzei K, Hata N, Haker SJ, Kacher DF, et al. Robot-assisted needle placement in open MRI: system architecture, integration and validation. *Comput Aided Surg.* 2007;12(1):15–24.
 52. Song SE, Cho NB, Iordachita I, Guion P, Fichtinger G, Whitcomb LL. A study of needle image artifact localization in confirmation imaging of MRI-guided robotic prostate biopsy. *IEEE Int Conf Robot Autom.* 2011;2011:4834–9.
 53. Song S, Cho N, Iordachita I, Guion P, Fichtinger G, Kaushal A, et al. Biopsy needle artifact localization in MRI-guided robotic transrectal prostate intervention. *IEEE Trans Biomed Eng.* 2012;59(7):1902–11.
 54. Blumenfeld P, Hata N, DiMaio S, Zou K, Haker S, Fichtinger G, Tempany C. MR-guided transperineal biopsy: needle placement accuracy study. *J Magn Reson Imaging.* 2007;26(3):688–94.
 55. Xu S, Kruecker J, Turkbey B, Glossop N, Singh AK, Choyke P, et al. Real-time MRI-TRUS fusion for guidance of targeted prostate biopsies. *Comput Aided Surg.* 2008;13:255–64.
 56. Turkbey B, Xu S, Kruecker J, Locklin J, Pang Y, Bernardo M, et al. Documenting the location of prostate biopsies with image fusion. *BJU Int.* 2011;107(1):53–7.
 57. Ukimura O, Hirahara N, Fujihara A, Yamada T, Iwata T, Kamoi K, et al. Technique for a hybrid system of real-time transrectal ultrasound with preoperative magnetic resonance imaging in the guidance of targeted prostate biopsy. *J Urol.* 2010;17(10):890–3.
 58. Chinzei K, Hata N, Jolesz FA, Kikinis R. MRI compatible surgical assist robot: system integration and preliminary feasibility study. In: *Lecture notes in computer science, Proc MICCAI*, vol. 1935. Pittsburgh: Springer; 2000. p. 921–30.
 59. Tsekos NV, Khanicheh A, Christoforou E, Mavroidis C. Magnetic resonance compatible robotic and mechatronics systems for image-guided interventions and rehabilitation. *Annu Rev Biomed Eng.* 2007;9:351–87.
 60. Elhawary H, Zivanovic A, Davies B, Lamprth M. A review of magnetic resonance imaging compatible manipulators in surgery. *Proc Inst Mech Eng H.* 2006;220:413–24.
 61. Kaiser WA, Fischer H, Vagner J, Selig M. Robotic system for biopsy and therapy of breast lesions in a high-field whole-body magnetic resonance tomography unit. *Invest Radiol.* 2000;35(8):513–9.
 62. Krieger A, Iordachita I, Guion P, Singh AK, Kaushal A, Menard C, Pinto PA, Camphausen K, Fichtinger G, Whitcomb LL. An MRI-compatible robotic system with hybrid tracking for MRI-guided prostate intervention. *IEEE Trans Biomed Eng.* 2011;58(11):3049–60.
 63. Hushek S, Fetis B, Moser R. Initial clinical experience with a passive electromagnetic 3D locator system. In: *Proceedings of the 5th interventional MRI symposium*. Boston; 15–16 Oct 2004.
 64. Dumoulin CL, Souza SP, Darrow RD. Real-time position monitoring of invasive devices using magnetic resonance. *Magn Reson Med.* 1993;29(3):411–5.
 65. Krieger A, Susil RC, Menard C, Coleman JA, Fichtinger G, Atalar E, Whitcomb LL. Design of a novel MRI compatible manipulator for image guided prostate interventions. *IEEE Trans Biomed Eng.* 2005;52(2):306–13.
 66. Hata N, Tokuda J, Morikawa S, Dohi T. Projection profile matching for intraoperative MRI registration embedded in MR imaging sequence. *Med Image Comput Comput Assist Interv.* 2002;2002:164–9.
 67. Tadayyon H, Lasso A, Gill S, Kaushal A, Guion P, Fichtinger G. Target motion tracking in MRI-guided transrectal robotic prostate biopsy. *IEEE Trans Biomed Eng.* 2011;58(11):3135–42.
 68. Ménard C, Susil RC, Choyke P, Coleman J, Grubb R, Gharib A, et al. An interventional magnetic resonance imaging technique for the molecular characterization of intraprostatic dynamic contrast enhancement. *Mol Imaging.* 2005;4(1):63–6.
 69. Singh AK, Guion P, Sears Crouse N, Ullman K, Smith S, et al. Simultaneous integrated boost of biopsy proven MRI defined dominant intra-prostatic lesions to 95 gray with IMRT: early results of a phase I NCI study. *Radiat Oncol.* 2007;18:2(1).
 70. Singh AK, Krieger A, Lattouf JB, Guion P, Grubb III RL, Albert PS, et al. Patient selection appears to determine prostate cancer yield of dynamic contrast enhanced MRI guided transrectal biopsies in a closed 3 Tesla scanner. *Br J Urol.* 2007;101(2):181–5.
 71. Wallner K, Dattoli MJ, Blasko J. *Prostate brachytherapy made complicated*, vol. 131. Seattle: Smart Press; 1997.
 72. Fischer G, Iordachita I, Csoma C, Tokuda J, DiMaio SP, Tempany CM, Hata N, Fichtinger G. MRI-compatible pneumatic robot for transperineal prostate needle placement. *IEEE/ASME Trans Mechatron.* 2008;13(3):3295–305.
 73. Seifabadi R, Song SE, Krieger A, Fichtinger G, Iordachita I. Robotic system for MRI-guided prostate biopsy: feasibility of teleoperated needle insertion and ex vivo phantom study. *Int J Comput Assist Radiol Surg.* 2012;7:181–90.
 74. Tadakuma K, DeVita LM, Dubowsky SY, Dubowsky S. The experimental study of a precision parallel manipulator with binary actuation: with application to MRI cancer treatment. In: *Proceeding of IEEE international conference on robotics and automation ICRA*. Pasadena; 2008. p. 2503–8.
 75. Stoianovici D, Song D, Petrisor D, Ursu D, Mazilu D, Muntener M, Mutener M, Schar M, Patriciu A. MRI stealth robot for prostate interventions. *Minim Invasive Ther Allied Technol.* 2007;16:241–8.
 76. Goldenberg AA, Trachtenberg J, Kucharczyk W, Yi Y, Haider M, Ma L, Weersink R, Raoufi C. Robotic system for closed-bore MRI-guided prostatic interventions. *IEEE/ASME Trans Mechatron.* 2008;13:374–9.
 77. Van den Bosch MR, Moman MR, V Vulpen M, Battermann JJ, Duiveman E, V Schelven LJ, D. Leeuw H, Lagendijk JJW, Moerland MA. MRI-guided robotic system for transperineal prostate interventions: proof of principle. *Phys Med Biol.* 2010;55(5):N133–40.
 78. Zangos S, Melzer A, Eichler K, Sadighi C, Thalhammer A, Bodelle B, et al. MR-compatible assistance system for biopsy in a high-field-strength system: initial results in patients with suspicious prostate lesions. *Radiology.* 2011;259(3):903–10.